J Mater Sci: Mater Electron (2015) 26:6450–6457
DOI 10.1007/s10854-015-3236-4

Inductive type properties of FeCoZr–CaF_2 and FeCoZr–PZT nanocomposites

Tomasz N. Koltunowicz[1]

Received: 10 January 2015 / Accepted: 22 May 2015 / Published online: 28 May 2015

Abstract The paper presents investigations into frequency dependences of conductivity, capacitance and the phase angle θ for nanocomposites $(FeCoZr)_x(CaF_2)_{(100-x)}$ and $(FeCoZr)_x(PZT)_{(100-x)}$. The nanocomposites have been produced with the application of ion-beam sputtering using pure argon ions (oxygen-free materials) and mixed ions of argon and oxygen (oxygen materials). The phase angle versus frequency characteristics for the oxygen nanocomposites show a transition from negative to positive phase angle values along with the frequency increase. The maximum observed phase angle θ values reach beyond the 90°. The phase angle transition through 0° is accompanied with the voltage resonance phenomenon that is represented by strong minima in the capacitance versus frequency curves. In the conductivity versus frequency characteristics, strong minima occur during the phase angle θ transition through 90°, which corresponds to the occurrence of current resonance. Occurrence of the coilless inductance features in nanocomposites $(FeCoZr)_x(PZT)_{(100-x)}$ and $(FeCoZr)_x(CaF_2)_{(100-x)}$, produced with the ion-beam sputtering using argon and oxygen ions, is related to the formation of a subsurface layer of metal oxides on the metallic phase nanogranules.

✉ Tomasz N. Koltunowicz
t.koltunowicz@pollub.pl

[1] Department of Electrical Devices and High Voltage Technology, Lublin University of Technology, 38d Nadbystrzycka Street, 20-618 Lublin, Poland

1 Introduction

Materials of the nanocomposite structure have drawn a lot of attention for the recent 20 years. Composites composed of ferromagnetic nanoparticles set in a dielectric matrix make an example of such materials. Matrices are the most often made of very stable dielectrics in the form of metal oxides such as Al_2O_3 [1–3] or SiO_2 [4–7] or of non-oxide dielectrics (oxygen-free matrices) like fluorides CaF_2 [8–10] as well as of ferroelectric materials PZT [11–13] or materials of low conductivity [14].

Such nanocomposites exhibit interesting electric [5, 8, 11, 12] and magnetic properties [15] together with higher values of many mechanical properties such as microhardness and tribological properties [14, 16] as well as higher corrosion resistance [17]. They present interesting optic and magneto-optic properties [18–21], high absorption coefficient of electromagnetic radiation within the range of radio and microwave frequency [4, 18, 22].

The paper presents a comparative analysis of AC properties of nanocomposites of the ferromagnetic alloy-ferroelectric $(FeCoZr)_x(PZT)_{(100-x)}$ structure and of the ferromagnetic alloy—dielectric $(FeCoZr)_x(CaF_2)_{(100-x)}$, structure produced with the ion-beam sputtering using pure argon ions (oxygen-free materials) or mixed argon and oxygen ions (oxygen materials).

Hopping of electron transport (tunnelling) between potential wells, which are located on nanometer distances from each other, causes that well, from which electron jumped, is charged positively, while the well to which electron jumped obtains a negative charge. It means there is further polarization of the material. For conductivity, caused by electron tunnelling between potential wells, an important parameter of phenomena is relaxation time τ. This is the time since creation of dipole to electron return

to the well, from which it started its jump. Relaxation time value have an important impact on conductivity value, which is caused by hopping of electron transport, and on frequency range, in which these phenomena occurs.

In paper [23] model of hopping of electron transport on DC an AC is presented. From the model results that in materials, with hopping conduction mechanism, in area of low values of angular frequency $\omega \ll 1/\tau$ conductivity is a constant value (DC conductivity). In intermediate frequency area $\omega \sim 1/\tau$ model predicts conductivity increase described by the formula:

$$\sigma(\omega) \propto \omega^{\alpha} \quad (1)$$

where $\sigma(\omega)$—conductivity; $\omega = 2\pi f$—angular frequency; f—frequency; α—frequency coefficient.

Value of frequency coefficient α depends on probability $(1 - p)$, with which electron after the jump from first to second well will return to first well. While value of probability p determines DC flow and DC conductivity value. This indicator shows, how many times DC conductivity is smaller than high-frequency conductivity. In high frequency area $(\omega > 1/\tau)$ conductivity ceases to grow and seeks to obtain a constant value.

Sum of the values of probabilities of jumps from second to first well $(1 - p)$ and probabilities of jump from second well to third p gives unity. It means that in the case, which was discussed in model, charge conservation law occurs.

2 Experimental

Nanocomposites $(FeCoZr)_x(CaF_2)_{(100-x)}$ and $(FeCoZr)_x(PZT)_{(100-x)}$, where the PZT acronym denotes a ferroelectric material of the composition $(Pb_{81}Sr_4(Na_{50}Bi_{50})_{15}(Zr_{57.5}Ti_{42.5}))O_3$, have been produced in a vacuum chamber at the pressure of about 1×10^{-3} Pa using ion-beam sputtering of the target composed of a ferromagnetic alloy $Co_{0.45}Fe_{0.45}Zr_{0.10}$ plate and dielectric strips affixed to the plate. The nanocomposites have been produced according to the method described in [24, 25]. A beam of pure argon ions (oxygen-free materials) and a beam of mixed argon and oxygen ions (oxygen materials) have been used for the sputtering purposes. Oxygen-free nanocomposites $(FeCoZr)_x(CaF_2)_{(100-x)}$ have been produced in the argon atmosphere at the pressure of $p_{Ar} = 1.1 \times 10^{-1}$ Pa, while the oxygen nanocomposites have been produced in the mixed argon-oxygen atmosphere at partial pressures of $p_{Ar} = 8.5 \times 10^{-2}$ Pa and $p_{O2} = 4.3 \times 10^{-3}$ Pa, respectively. Due to low stability of the structure, at the production of the nanocomposites $(FeCoZr)_x(PZT)_{(100-x)}$, the compounds cannot be obtained in the atmosphere of pure argon. The structures have been produced using combined beams of argon with a minimal oxygen content ($p_{Ar} = 7.4 \times 10^{-2}$ Pa and $p_{O2} = 5\times10^{-3}$ Pa) and with a high oxygen content ($p_{Ar} = 6.6 \times 10^{-2}$ Pa and $p_{O2} = 3\times10^{-3}$ Pa). The ion energy has been of about 5 keV.

We have also used a SEM LEO1455-VP with an energy-dispersive Si:Li detector Rontec to perform an X-Ray microanalysis for x checking with the accuracy of ~ 1 %.

Before the electric properties study, a structural characterization of the films was carried out basing on the results of transmission electron microscopy (TEM, Philips EM400T and Philips CM200), X-ray diffraction (XRD, PANalytical diffractometer, Cu K_α) and ^{57}Fe transmission electron Mössbauer spectroscopy (20 mCi ^{57}Co in Rh source). As was previously shown in [9, 26], $(FeCoZr)_x(CaF_2)_{(100-x)}$ nanocomposites are of a granular structure with an average size of the ferromagnetic alloy grain of about 3–5 nm. Corresponding TEM images are presented in Fig. 1.

As can be concluded from electron diffraction (ED) (see inserts in Fig. 1), individual rings characterizing metallic nanoparticles and CaF_2 matrix are detected, i.e. clear phase separation is evident for films synthesized in both atmospheres. This result is also confirmed by XRD data presented in Fig. 2 and described in details in [26, 27]. Both XRD and electron diffraction reveal that nanoparticles are characterized by *bcc* structure of FeCo alloy which is labeled as α-FeCo(Zr) [9, 26, 28]. XRD detects nanoparticles disordered structure because only few broad peaks from α-FeCo(Zr) are on XRD patterns of films with $x = 29$–65 at.%.

It should be mentioned, that $(FeCoZr)_x(CaF_2)_{(100-x)}$, $36 \le x \le 74$, films obtained in argon-oxygen atmosphere demonstrate additional diffraction peak (ring) from oxide phase marked in Figs. 1 and 2 as a-$(Fe,Co,Zr)_xO_y$. Since it is possible to detect only one broad peak on XRD-pattern (single ring on ED image) from a-$(Fe,Co,Zr)_xO_y$ oxide, it is impossible to identify its phase composition exactly. Probably, the oxide dislocates at nanoparticles surface and forms "metallic core—oxide shell" structures, as it was previously proved for $(FeCoZr)_x(Al_2O_3)_{(100-x)}$ films synthesized by the same method and under the same conditions (p_{O2}) [28, 29].

Direct observation of FeCoZr-based nanoparticles inside PZT matrix is experimentally more complicated than in the cases of CaF_2 matrix (or Al_2O_3). The reason is that matrix and nanoparticles both contain heavy elements (Zr, Ti) and cannot be clearly separated by TEM. However, combination of techniques (Mössbauer spectroscopy, Raman spectroscopy, XRD, X-ray absorption) clearly reveals the formation of well-separated α-FeCo(Zr), FeCo-based oxides and PZT-like phases in films [11, 30–32]. Mössbauer spectra of $(FeCoZr)_x(PZT)_{(100-x)}$ films synthesized in atmospheres with two different oxygen pressures are shown in Fig. 3.

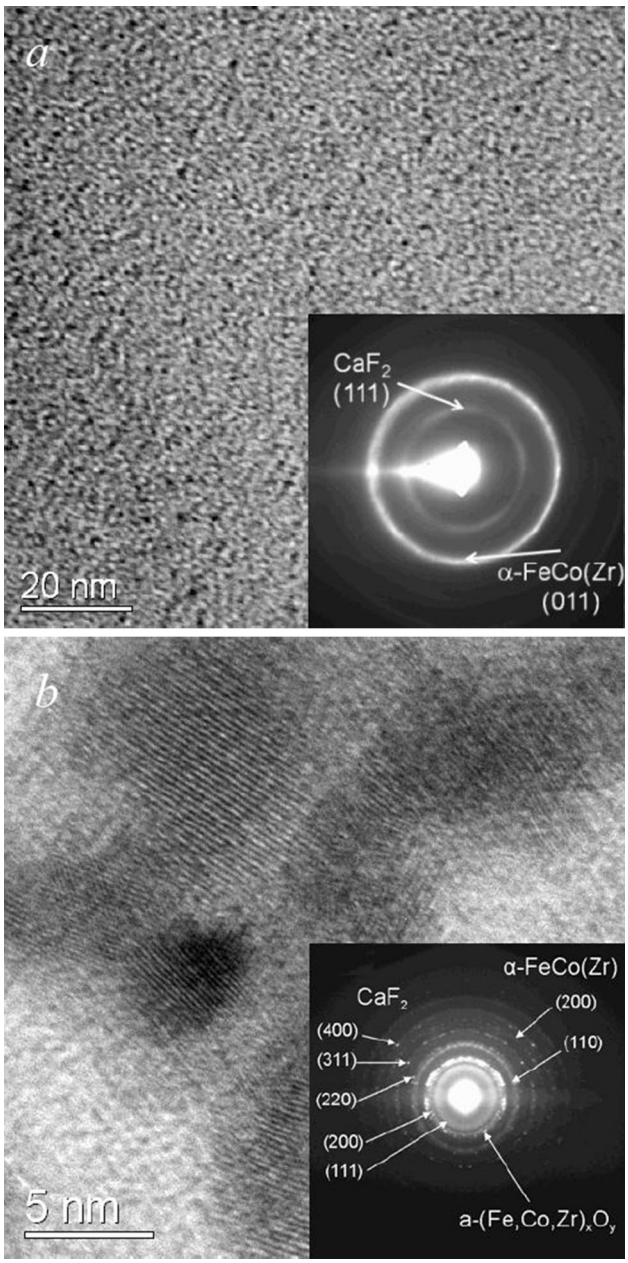

Fig. 1 TEM imades of $(FeCoZr)_{39}(CaF_2)_{61}$ film obtained in Ar atmosphere (**a**) and $(FeCoZr)_{36}(CaF_2)_{64}$ film obtained in argon-oxygen atmosphere (**b**); the *inserts* present electron diffraction of the films

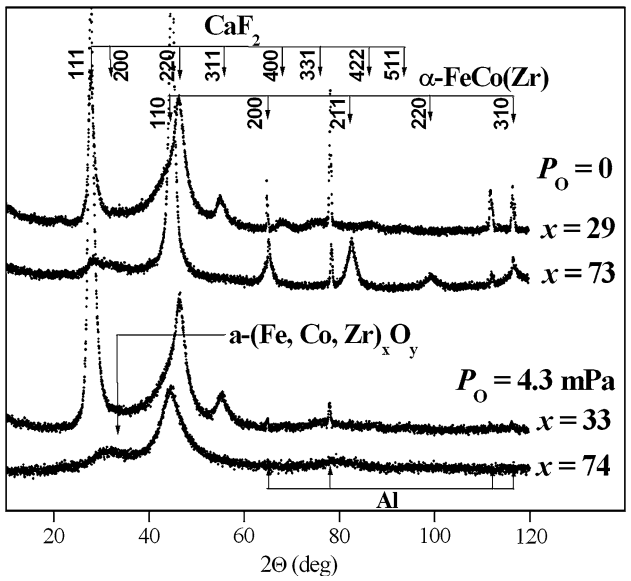

Fig. 2 XRD patterns of $(FeCoZr)_x(CaF_2)_{100-x}$ ($x = 29$–74) films obtained in argon (*top panel*) and argon-oxygen (*bottom panel*) atmosphere [27]

Mossbauer spectrum of $(FeCoZr)_{50}(PZT)_{50}$ film obtained in atmosphere with lower oxygen pressure $p_{O2} = 2.4 \times 10^{-3}$ Pa (Fig. 3a) demonstrates full nanoparticles oxidation. It consists of two doublets characterizing different types of oxides, namely $Fe(Co)_3O_4$ or $Fe(Co)_2O_3$ (characterized with the superparamagnetic doublet, $\delta = 0.3$–0.45 mm/s, $\Delta E = 0.9$–1.2 mm/s for different x), and $(Fe_xCo_{1-x})_{1-\delta}O$ (characterized with the doublet, $\delta = 0.9$-1.1 mm/s, $\Delta E = 1.7$–1.8 mm/s) [11, 30, 31]. However, XRD of the film (see insert in upper Fig. 3a) detects also a diffraction line of low intensity from α-FeCo(Zr) structure in addition to the peaks characterizing PZT-matrix and FeCo-based oxide. This means that FeCoZr-based nanoparticles in a PZT-matrix can form metallic "core—oxide shell" structure [11, 31] typically observed for the FeCoZr-alumina nanocomposites [28, 29]. The main diffraction peaks from PZT-matrix and FeCo-based oxide cannot be clearly separated from each other because of their close position ($2\Theta \sim 31$–$33°$). However, strong asymmetry of the detected peak at $2\Theta \sim 32°$ increasing with x allows to conclude the phase separation.

Increase of FeCoZr concentration to $x \geq 67$ at.% leads to appearance of additional sextet on Mössbauer spectra (Fig. 3a) characterizing ferromagnetic metallic α-FeCo(Zr) nanoparticles (or their agglomerations). This is accompanied with the significant increase of α-FeCo(Zr) peak intensity on XRD pattern of the studied film (insert in lower Fig. 3a). Some displacement of XRD peak characterizing both PZT-matrix and FeCo-based oxides to higher 2Θ values indicates the increase of FeCo-based oxides contribution with respect to PZT phase.

$(FeCoZr)_x(PZT)_{(100-x)}$ films synthesized at higher oxygen pressure of $p_{O2} \geq 3.7 \times 10^{-3}$ Pa contain fully oxidized superparamagnetic nanoparticles of either $Fe(Co)_3O_4$ or $Fe(Co)_2O_3$ oxides over the whole range of studied x ($x = 35$–81 at.%) [30–32]. This is confirmed by Mössbauer spectra shown in Fig. 3b for $x = 43$ and 67 at.%. Both spectra are characterized by the similar doublets with $\delta \sim 0.3$ mm/s, $\Delta E = 1.0$ mm/s. XRD analysis also proves the absence of non-oxidized α-FeCo(Zr) phase in $(FeCoZr)_x(PZT)_{(100-x)}$ films obtained at higher oxygen

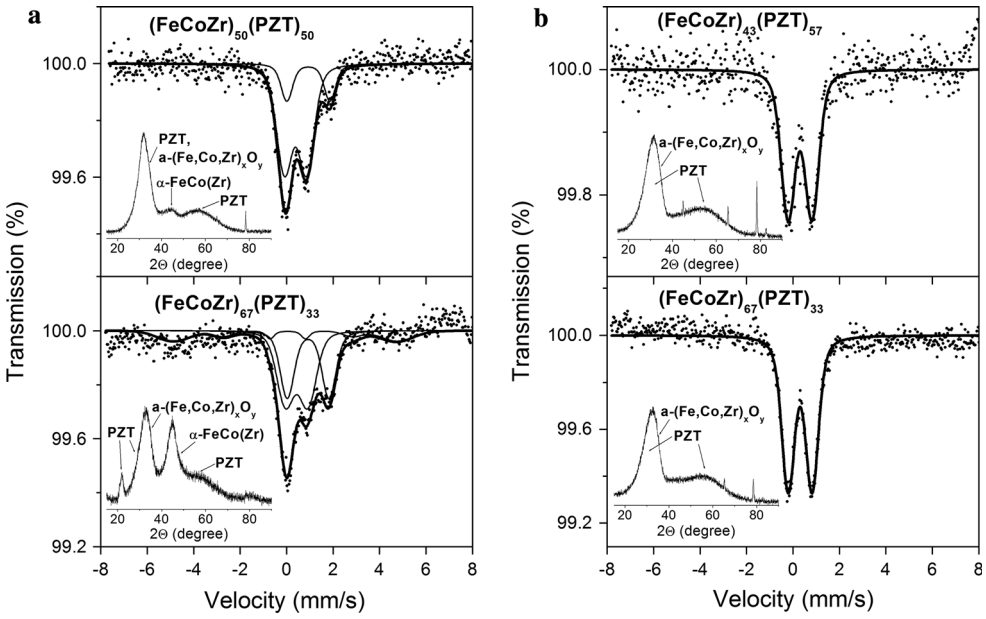

Fig. 3 Mossbauer spectra of $(FeCoZr)_x(PZT)_{(100-x)}$, $x = 50$ and 67 at.%, films obtained in atmosphere with lower oxygen pressure ($p_{O2} = 2.4$ mPa) (**a**) and $(FeCoZr)_x(PZT)_{(100-x)}$, $x = 43$ and 67 at.%, films obtained in atmosphere with higher oxygen pressure ($p_{O2} = 3.7$ mPa) (**b**); the *inserts* present XRD patterns of the films

pressure (see inserts in Fig. 3b). Thus, these films consist of a-$(Fe,Co,Zr)_xO_y$ granules in PZT-matrix.

Testing of the electric properties has been performed at the AC, within the frequency range of 50 Hz –1 MHz. Measurements have been made for the resistance R_p and capacitance C_p in a parallel equivalent circuit as well as for the phase angle θ. Electric parameters have been measured using the measuring temperature range T_p from 77 K to 373 K at the temperature change step of 5 K. Component meters of the test stand are computer-connected and controlled by a program written in the Visual C++ software environment. Measurement results are saved in the computer memory.

Samples have been subjected to the 15-min annealing in a tubular furnace controlled with a thermoregulator, in the temperature T_a of 398 K and higher at the temperature interval step of 25 K. Temperature has been maintained with the accuracy of ±1 K.

3 Comparison of the AC properties of oxygen-free and oxygen nanocomposites

Figure 4 presents frequency dependences of the phase angle θ for a nanocomposite $(FeCoZr)_x(PZT)_{(100-x)}$, produced with the sputtering using argon ions with a minimal content of oxygen, of the metallic phase content $x = 51.7$ at.%, annealed in the temperature of 548 K. Figure 4 shows selected example curves obtained for four out of 63 measuring temperatures T_p.

As can be seen in Fig. 4a, in a low frequency area negative values of the phase angle θ occur, which means that capacitive conduction is a dominating type of conductivity there. Frequency increase makes the phase angle reach its minimum at a certain frequency value and then causes its further growth. It should be noted that over the whole examined frequency range the phase angle values remain negative. Conductivity (Fig. 4b) in the low (to about 500 Hz) and high (more than 50 kHz) frequency areas remains almost constant, while for the medium frequency range of 500 Hz $< f <$ 50 kHz, conductivity rapidly increases along with the frequency increase. Such conductivity behaviour is characteristic for the hopping exchange of electric charges between metallic-phase nanoparticles and is consistent with the hopping carrier transport model on DC and AC [2, 9, 11]. In Fig. 4c it can be seen that in the low frequency area, capacitance (dielectric permittivity) remains constant. When frequency further increases and exceeds the value of f_0, that approaches the inverse relaxation time τ, rapid decrease of capacitance occurs. Temperature dependence on permittivity can also be observed and specifically its increase along with the temperature growth. This is consistent with a model of thermally activated permittivity that is characteristic for the hopping exchange of electric charges [33, 34].

In the case when the ion beam applied to the nanocomposite production includes argon ions and a high content of oxygen (oxygen materials), frequency dependences of θ, σ and C_p for nanocomposites of a similar metallic phase content (52.0 at.%) are considerably differ. As can be seen in Fig. 5a, the phase angle θ changes from negative values in the low frequency area to the values higher than 90° in the high frequency area. Figure 5b presents dependencies of conductivity as a function of the frequency and shows that at the phase angle θ (Fig. 5a)

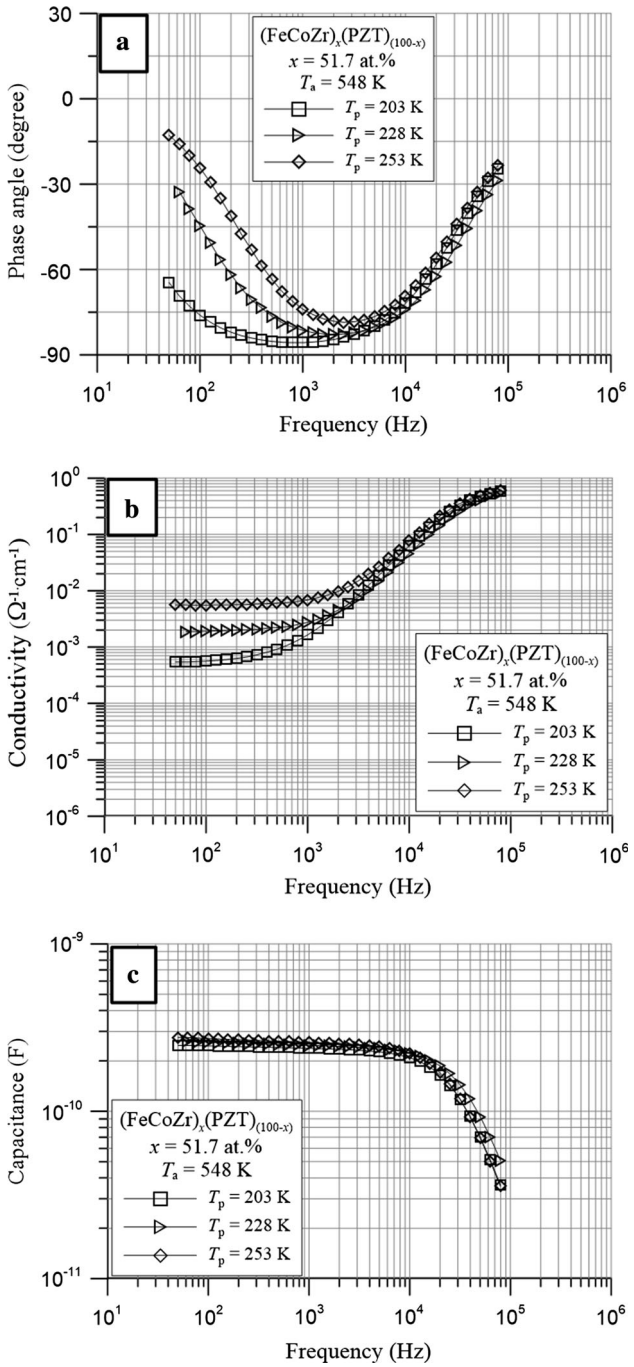

Fig. 4 Frequency dependences of the **a** phase angle θ, **b** conductivity, **c** capacitance for a nanocomposite $(FeCoZr)_x(PZT)_{(100-x)}$ of the metallic phase content $x = 51.7$ at.%, produced with the sputtering using argon ions with a minimal oxygen content and annealed in the temperature of 548 K. Measuring temperatures T_p: *1*—203 K, *2*—228 K, *3*—253 K

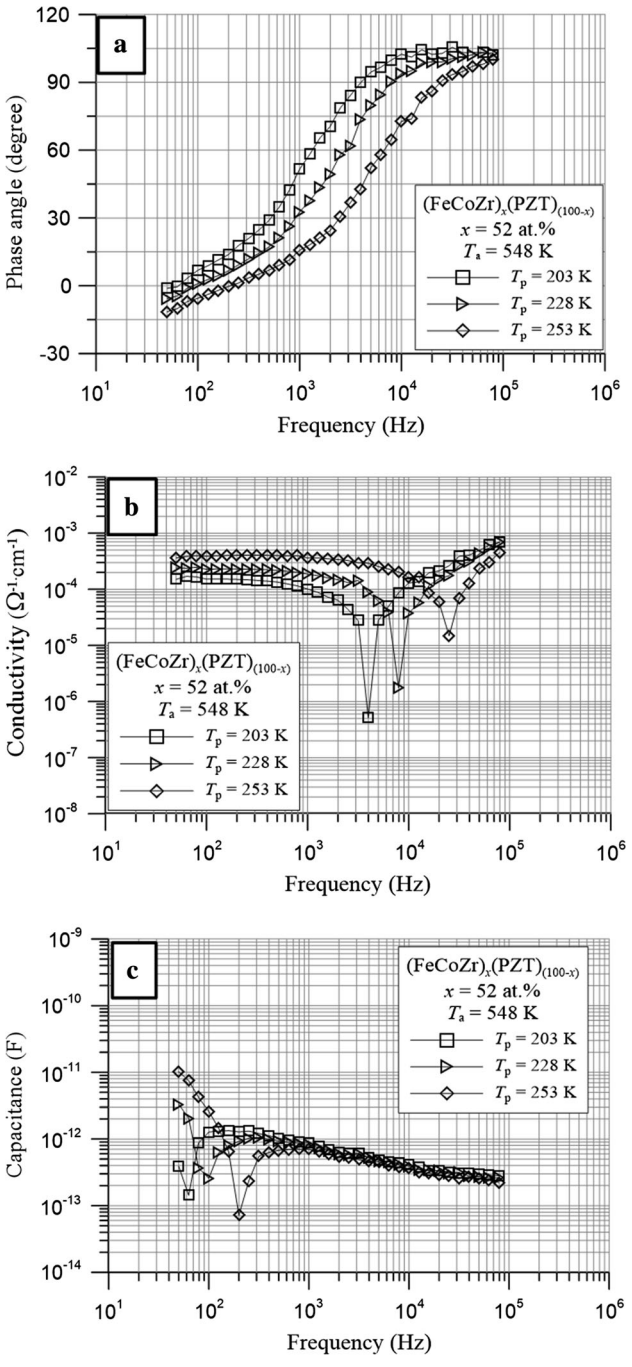

Fig. 5 Frequency dependences of the **a** phase angle θ, **b** conductivity, **c** capacitance for a nanocomposite $(FeCoZr)_x(PZT)_{(100-x)}$ of the metallic phase content $x = 52.0$ at.%, produced with the sputtering using argon ions with a high content of oxygen and annealed in the temperature of 548 K. Measuring temperatures T_p: *1*—203 K, *2*—228 K, *3*—253 K

transition through 0° in the C_p characteristic a strong minimum occurs (Fig. 4c), which is related to the occurrence of voltage resonance. Mutual compensation of capacitive and inductive voltage components takes place, which is expressed by the measured value of capacitance approaching zero. At the phase angle transition θ through 90° (Fig. 5c) current resonance occurs, which corresponds to the occurrence of a strong minimum in the conductivity versus frequency curve.

In this nanocomposite (Fig. 5) a phenomenon of the coilless inductance occurs. The phenomenon consists in that in a layer where there are no windings (no coil), the phase angle values are positive, which is characteristic for inductance.

Coilless inductance advantage is the ability to use a thin layer of the nanocomposite to shift the phase angle in the area of positive values. In conventional circuits for this purpose coils are used.

From Fig. 5 results that the temperature increase causes shift of minimums, which are located on dependence $C_p(f)$ and correspond to frequency of voltage resonance ($\theta = 0°$), in higher temperatures area. Similar situation is observed for minimums on dependence $\sigma(f)$—it is current resonance ($\theta = 90°$). It is related to temperature changes of time τ.

Figure 6a presents frequency dependences of the phase angle for a nanocomposite $(FeCoZr)_x(CaF_2)_{(100-x)}$ produced with the ion-beam sputtering using pure argon ions (oxygen-free material). As can be seen, over the whole range of the measured frequency, the phase angle values are negative (capacitive type of conduction). Conductivity curve shown in Fig. 6b exhibits two increase segments separated by a segment of an almost constant value. It means that conduction in that material is realized by hopping exchange of electric charges and that in the material there are two types of potential wells for the electrons to hop between them. It can also be seen in the $C_p(f)$ curve of Fig. 6c, where two segments of the decreasing capacitance occur. It indicates that in the material two types of potential wells occur and they differ by the relaxation times. The maximum, that can be seen in the dependence $\theta(f)$ (Fig. 6a), is also related to the two types of potential wells.

Figure 7 presents frequency dependences of the phase angle, conductivity and capacitance for a nanocomposite $(FeCoZr)_x(CaF_2)_{(100-x)}$, produced with the ion-beam sputtering using argon and oxygen ions (oxygen material) of the metallic phase content as in the previous case of the oxygen-free sample, that is $x = 62.7$ at.%. For the oxygen material, the obtained dependences $\theta(f)$, $\sigma(f)$ and $C_p(f)$ resemble the ones obtained for the nanocomposite $(FeCoZr)_x(PZT)_{(100-x)}$ produced with the ion-beam sputtering using argon and oxygen ions. In this case, the coilless inductance phenomenon can also be observed. It consists in the occurrence of the phase angles of positive value. In this material current resonance occurs at the phase angle θ transition through the value of 90° and voltage resonance occurs when $\theta = 0°$, which can be seen in the form of sharp minima in Fig. 7b, c.

In Fig. 7 it can be observed that on frequency dependences on conductivity and capacity minimums shift (related to voltage and current resonances) in area of higher frequencies occurs together with temperature increase.

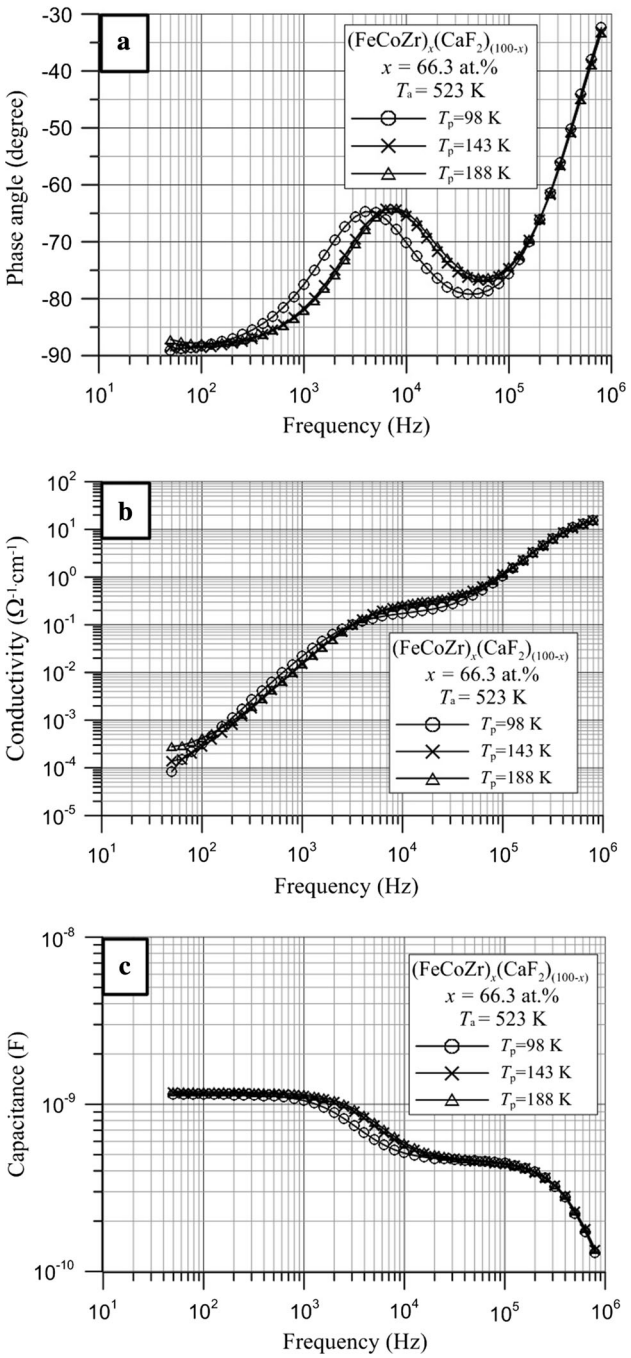

Fig. 6 Frequency dependences of the **a** phase angle θ, **b** conductivity; **c** capacitance for nanocomposite $(FeCoZr)_x(CaF_2)_{(100-x)}$ with metallic phase content $x = 66.3$ at.%, produced by produced by sputtering using pure argon ions and annealed in temperature 523 K. Measurement temperatures T_p: *1*—98 K, *2*—143 K, *3*—188 K

There is no doubt, that the lack of positive phase angle values in the oxygen-free nanocomposites and in the nanocomposites with an insignificant oxygen content as well as their occurrence in the oxygen materials is related to the presence of oxygen in the sputtering beam. It follows from the results of our previous investigations on the

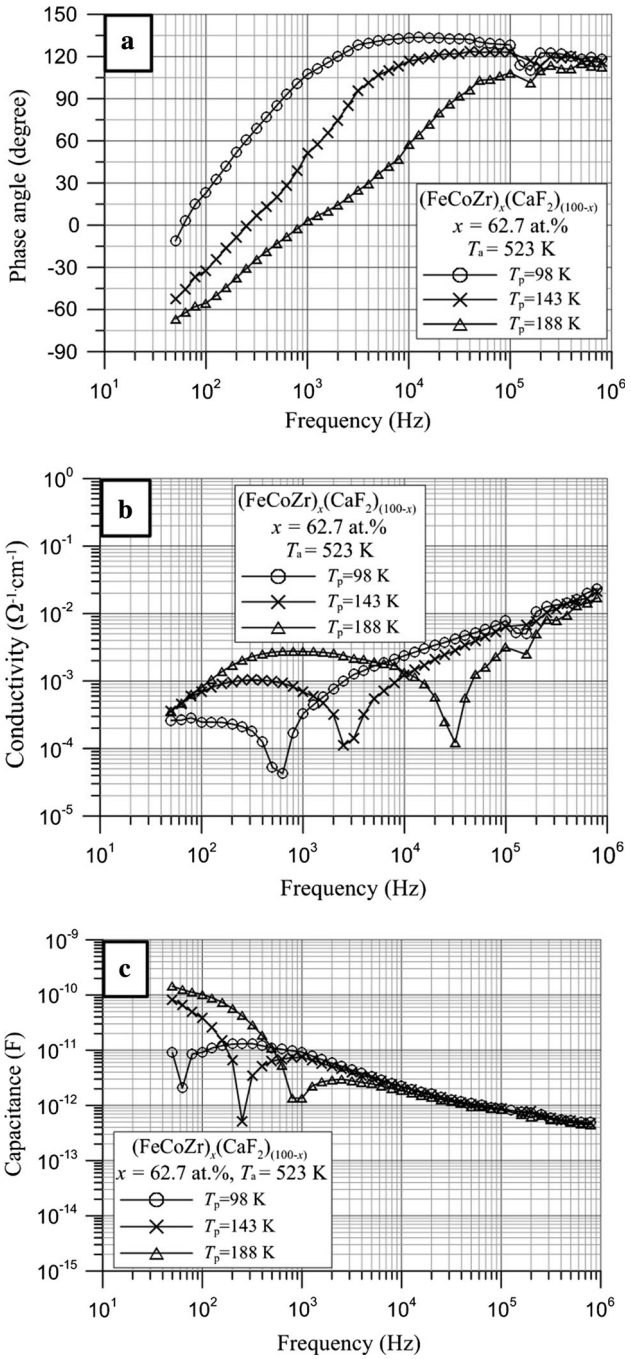

Fig. 7 Frequency dependences of the **a** phase angle θ, **b** conductivity, **c** capacitance for a nanocomposite $(FeCoZr)_x(CaF_2)_{(100-x)}$ of the metallic phase content $x = 62.7$ at.%, produced by with the ion beam sputtering using argon and oxygen ions and annealed in the temperature of 523 K. Measuring temperatures T_p: *1*—98 K, *2*—143 K, *3*—188 K

coilless inductance phenomenon in the oxygen nanocomposites $(FeCoZr)_x(Al_2O_3)_{(100-x)}$ that the occurrence of this phenomenon is related to the formation of a coating of metal oxides on the metallic-phase nanogranule surfaces [2, 3]. The occurrence of the coilless inductance phenomenon in nanocomposites $(FeCoZr)_x(PZT)_{(100-x)}$ and $(FeCoZr)_x(CaF_2)_{(100-x)}$, produced with the ion-beam sputtering using argon and oxygen ions, indicates that also in this materials on the nanogranule surfaces a film of metal oxides forms. That oxide layer makes a double barrier, and electrons hop through it (tunnelling) on their way from one metallic nanogranule core to another, the cores making the potential wells.

As was established in the works [10, 11, 31] in nanocomposites ferromagnetic alloy—dielectric electron hopping occurs between metallic phase nanoparticles, which are close to each other. Whereas electron hopping with variable jumps distance, which occurs at the temperature of liquid helium, is rather impossible because of the high measurement temperatures about 80 K and higher.

4 Conclusions

The paper presents an analysis of frequency dependences of conductivity, capacitance and the phase angle θ for nanocomposites $(FeCoZr)_x(CaF_2)_{(100-x)}$ and $(FeCoZr)_x(PZT)_{(100-x)}$. The nanocomposites have been produced with the ion-beam sputtering technique using of pure argon ions (oxygen-free materials) and mixed argon and oxygen ions (oxygen materials). In the oxygen-free materials the phase angle occurs in the negative value area (capacitive type of conduction).

On the other hand, for the oxygen nanocomposites, in the phase angle versus frequency dependences a transition from the negative (capacitive type of conduction) to positive (inductive type of conduction) values that occurs along with the frequency increase can be observed. The observed maximum values of phase angle θ exceed the 90°. The phase angle θ transition through 0° is accompanied by voltage resonance that can be seen as strong minima on the capacitance versus frequency characteristics, at the phase angle θ transition through 90°, which corresponds to the current resonance occurrence.

The coilless inductance in the nanocomposites $(FeCoZr)_x(PZT)_{(100-x)}$ and $(FeCoZr)_x(CaF_2)_{(100-x)}$, produced with the ion-beam sputtering using argon and oxygen ions is related to the formation of a subsurface film of metal oxides on the metallic-phase nanogranules is occur. This film creates double barrier, through which electrons jump (tunnelling) on the way from first to second nanogranule metallic core, which are potential wells.

Acknowledgments This research was carried out in the framework of the research project No. IP 2012 026572 from the Iuventus Plus program of the Polish Ministry of Science and Higher Education in the years 2013–2015.

References

1. A.D. Pogrebnjak, A.P. Shpak, G.V. Kirik, N.K. Erdybaeva, M.V. Il'yashenko, A.A. Dem'yanenko, Y.A. Kunitskii, A.S. Kaverina, V.S. Baidak, N.A. Makhmudov, P.V. Zukowski, F.F. Komarov, V.M. Beresnev, S.M. Ruzimov, A.P. Shypylenko, Acta Phys. Pol. A **120**(1), 94 (2011)
2. I. Svito, J.A. Fedotova, M. Milosavljević, P. Zhukowski, T.N. Koltunowicz, A. Saad, K. Kierczynski, A.K. Fedotov, J. Alloys Compd. **615**, S344 (2014)
3. P. Zhukowski, T.N. Kołtunowicz, P. Węgierek, J.A. Fedotova, A.K. Fedotov, A.V. Larkin, Acta Phys. Pol. A **120**(1), 43 (2011)
4. L. Deng, Z. Feng, J. Jiang, H. He, J. Magn. Magn. Mater. **309**, 285 (2007)
5. I. Svito, A.K. Fedotov, T.N. Koltunowicz, P. Zhukowski, Y. Kalinin, A. Sitnikov, K. Czarnacka, A. Saad, J. Alloys Compd. **615**, S371 (2014)
6. S. Honda, T. Okada, M. Nawate, M. Tokumoto, Phys. Rev. B **56**, 14566 (1997)
7. S. Honda, T. Okada, M. Nawate, J. Magn. Magn. Mater. **165**, 153 (1997)
8. T.N. Koltunowicz, P. Zhukowski, V. Bondariev, A. Saad, J.A. Fedotova, A.K. Fedotov, M. Milosavljevic, J.V. Kasiuk, J. Alloys Compd. **615**, S361 (2014)
9. T.N. Koltunowicz, P. Zukowski, M. Milosavljević, A.M. Saad, J.V. Kasiuk, J.A. Fedotova, YuE Kalinin, A.V. Sitnikov, A.K. Fedotov, J. Alloys Compd. **586**, S353 (2014)
10. T.N. Kołtunowicz, P. Zhukowski, V. Bondariev, J.A. Fedotova, A.K. Fedotov, Acta Phys. Pol. A **123**(5), 932 (2013)
11. T.N. Kołtunowicz, J.A. Fedotova, P. Zhukowski, A. Saad, A. Fedotov, J.V. Kasiuk, A.V. Larkin, J. Phys. D Appl. Phys. **46**(12), 125304 (2013)
12. T.N. Kołtunowicz, P. Zhukowski, A.K. Fedotov, A.V. Larkin, A. Patryn, B. Andriyevskyy, A. Saad, J.A. Fedotova, V.V. Fedotova, Elektronika ir Elektrotechnika (Electron. Electr. Eng.) **19**(4), 37 (2013)
13. A.V. Larkin, A.K. Fedotov, J.A. Fedotova, T.N. Koltunowicz, P. Zhukowski, Mater. Sci. Pol. **30**(2), 75 (2012)
14. A.D. Pogrebnjak, M.M. Danilionok, V.V. Uglov, N.K. Erdybaeva, G.V. Kirik, S.N. Dub, V.S. Rusakov, A.P. Shypylenko, P.V. Zukovski, Y.Z. Tuleushev, Vacuum **83**, S235 (2009)
15. P. Zhukowski, J. Sidorenko, T.N. Kołtunowicz, J.A. Fedotova, A.V. Larkin, Przeglad Elektrotechniczny **86**(7), 296 (2010)
16. A.D. Pogrebnjak, V.M. Beresnev, *Nanocoatings Nanosystems Nanotechnologies* (Bentham Science Publishers, Oak Park, IL, 2012)
17. F. Noli, P. Misaelides, A. Hatzidimitriou, E. Pavlidou, A.D. Pogrebnjak, Appl. Surf. Sci. **252**(23), 8043 (2006)
18. H.P. Khan, A. Granovsky, F. Brouers, E. Ganshina, J.P. Clerc, M. Kurmichev, J. Magn. Magn. Mater. **183**(1–2), 127 (1998)
19. Y.E. Kalinin, A.V. Sitnikov, O.V. Stognei, I.V. Zolotukhin, P.V. Neretin, Mater. Sci. Eng. A **304–306**, 941 (2001)
20. Y.H. Tang, X.M. Chen, Y.J. Li, X.H. Zheng, Mater. Sci. Eng. B **116**, 150 (2005)
21. Q. Wan, T.H. Wang, C.L. Lin, Nanotechnology **14**, L15 (2003)
22. K. Yakushiji, S. Mitani, K. Takanashi, J.G. Ha, H. Fujimori, J. Magn. Magn. Mater. **212**, 75 (2000)
23. P. Zukowski, T. Koltunowicz, J. Partyka, P. Wegierek, F.F. Komarov, A.M. Mironov, N. Butkievith, D. Freik, Vacuum **81**(10), 1137 (2007)
24. Y.E. Kalinin, A.T. Ponomarenko, A.V. Sitnikov, O.V. Stogney, Phys. Chem. Mater. Treat. **5**, 14 (2001)
25. I.V. Zolotukhin, Y.E. Kalinin, A.T. Ponomarenko, V.G. Shevchenko, A.V. Sitnikov, O.V. Stognei, O. Figovsky, J. Nanostruct. Polym. Nanocompos. **2**, 23 (2006)
26. J.V. Kasiuk, J.A. Fedotova, J. Przewoznik, J. Zukrowski, M. Sikora, Cz Kapusta, A. Grce, M. Milosavljević, J. Appl. Phys. **116**, 044301-1 (2014)
27. J.V. Kasiuk, J.A. Fedotova, T.N. Koltunowicz, P. Zukowski, A.M. Saad, J. Przewoznik, Cz Kapusta, J. Zukrowski, I.A. Svito, J. Alloys Compd. **586**(Supplement 1), S432 (2014)
28. J. Przewoznik, C. Kapusta, M. Milosavljevic, YuV Kasiuk, J. Zukrowski, M. Sikora, A.A. Maximenko, D. Szepietowska, K.P. Homewood, J. Phys. D Appl. Phys. **44**, 495001-1 (2011)
29. J. Fedotova, J. Kasiuk, J. Przewoznik, Cz Kapusta, I. Svito, Yu. Kalinin, A. Sitnikov, J. Alloys Compd. **509**, 9869 (2011)
30. YuV Kasyuk, J.A. Fedotova, M. Marszalek, A. Karczmarska, M. Mitura-Nowak, YuE Kalinin, A.V. Sitnikov, Solid State Phys. **54**(1), 178 (2012)
31. T.N. Koltunowicz, P. Zukowski, O. Boiko, A. Saad, J.A. Fedotova, A.K. Fedotov, A.V. Larkin, J. Kasiuk, J. Electron. Mater. (2015). doi:10.1007/s11664-015-3685-9
32. J.A. Fedotova, Acta Phys. Pol. A **125**(6), 1418 (2014)
33. P.W. Zukowski, A. Rodzik, Y.A. Shostak, Semiconductrors **31**(6), 610 (1997)
34. P.W. Zukowski, S.B. Kantorow, K. Kiszczak, D. Maczka, V.F. Stelmakh, A. Rodzik, E. Czarnecka-Such, Phys. Status Solidi A Appl. Res. **128**(2), K117 (1991)